ACS APPLIED MATERIALS & INTERFACES

www.acsami.org

Research Article

Multifunctional Additives for High-Energy-Density Lithium-Ion Batteries: Improved Conductive Additive/Binder Networks and Enhanced Electrochemical Properties

Junho Ahn, Byeongho Park, Jongsoon Kim, Moon-Kwang Um, Jin Woo Yi,* and Jung-Keun Yoo*

Cite This: *ACS Appl. Mater. Interfaces* 2021, 13, 19970−19982

Read Online

ACCESS | Metrics & More | Article Recommendations | Supporting Information

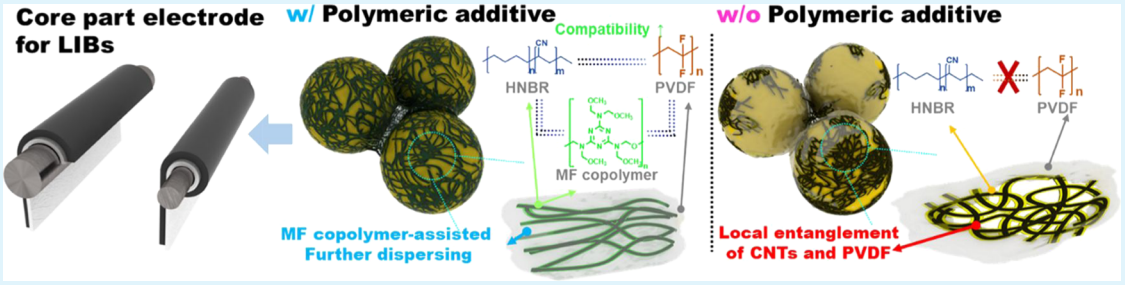

ABSTRACT: Cylindrical-type cells have been widely adopted by major battery and electric vehicle manufacturers owing to their price competitiveness, safety, and easy expandability. However, placement of electrodes at the core of cylindrical cells is currently restricted because of high electrode curvature and the lack of specialized electrodes and electrode materials. Here, we report the realization of highly flexible high-energy-density electrodes (active material loading of >98.4%) that can be used at the cores of cylindrical cells. The improved properties result from the introduction of a multifunctional poly(melamine-*co*-formaldehyde) (MF copolymer) additive, which yields a relatively more fluidic and well-dispersed slurry using only 0.08 wt %. MF copolymer-mediated formation of completely wrapped CNT/PVDF networks on $LiCoO_2$ (LCO) and accompanying contact enhancement between LCO and carbon nanotubes (CNTs) resulted in an increase of electrical and mechanical properties of the two types (composites with or without collectors) of electrodes compared with those of additive-free electrodes. Flexibility tests were carried out by rolling electrodes onto cylinder substrates (diameters of ca. 1 and 10 mm); this process resulted in relatively lower resistance changes of the MF copolymer-containing electrodes than for the reference electrodes. In addition, capacity retention after 100 cycles for cells with and without MF copolymers was approximately 10−20% better for the samples with the MF copolymer than for those without. CNT/PVDF networks with MF copolymers were proven to induce a relatively thin and stable cathode electrolyte interface layer accompanying the chemical bond formation during cycling.

KEYWORDS: *lithium-ion batteries, high-energy-density electrodes, conductive additive/binder networks, composite interfaces, electrode additives*

INTRODUCTION

The demand for lithium-ion batteries (LIBs) in electric vehicles (EVs) continues to grow, and the development of high-energy-density batteries is needed for further extension of the operation time and driving range of EVs. Battery manufacturers have adopted different types of cells, including cylindrical, prismatic, and pouch cells, designing them to meet the requirements of their customers.[1] Cylindrical-type 18650, 2170, and 4680 cells, despite their relatively low energy density, have been widely adopted by major battery and EV manufacturers such as Tesla because of their price competitiveness, standardized battery size, verified safety, and easy expandability.[2−5]

Cylindrical-type cells, including ca. 21 and 26 of wound electrodes for the 18650 and 2170 cells, respectively, are needed to maximize the energy density by investigating and developing specialized electrodes and electrode materials.[6−13] The materials and chemistry of the electrode for practical cylindrical cells are not very different from those of prismatic and stack-type cells. However, high curvature of a cylindrical cell can lead to separation and cracking of an electrode placed at its core, when the electrode has a diameter of less than ca. 2−3 mm.[3,6] To overcome this issue, it is necessary to improve the electrode flexibility through innovation and development at

Received: January 14, 2021
Accepted: April 9, 2021
Published: April 21, 2021

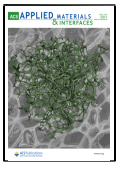

https://doi.org/10.1021/acsami.1c00848
ACS Appl. Mater. Interfaces 2021, 13, 19970−19982

the materials level. Previous studies have demonstrated that further development of inactive materials such as conductive additives and binders is critical to improve electrode flexibility.[14,15] For example, the incorporation of flexible and elastic binders can effectively increase the electrode flexibility.[16] In addition, well-known elastic polymers, such as polystyrene−polyisoprene−polystyrene (SIS) and polydimethylsiloxane (PDMS), have been used as binders for wearable rechargeable batteries.[17,18] Highly cross-linkable supramolecular polymers, such as polyacrylic acid (PAA) and polyethylene oxide (PEO)-based polyrotaxane or 2-ureido-4-pyrimidone (UPy), have also been applied as elastic binders for LIBs.[19,20] Moreover, as alternatives to conventional carbon black, conductive additives with a high aspect ratio (>10,000) and theoretical electrical conductivity (5×10^5 S/m for purified materials), such as carbon nanotubes (CNTs), have been shown to be very effective at improving the mechanical properties of electrodes by interconnecting the electrode components over a long range.[21−23] However, reported studies on importance of conductive materials/binder networks for electrode flexibilities in LIBs do not possess potential for practical applications.[14−20] Major issues among the interrupting factors are originated from the low areal active materials and mass loading of electrode layers as well as instabilities of slurry under bulk scale processing. Processing in the subgram scale for electrodes with an active materials loading of 80 wt % and a mass loading of 1−8 mg/cm^2 does not guarantee their electrochemical performances when they are applied to practical slurry and electrode formulations.

Therefore, a main challenge to be overcome to increase the electrode flexibility of practical cylindrical cells at their core parts is to optimize existing nonactive materials, i.e., binders and conductive materials, while minimizing their presence to less than 2 wt % in the electrode to improve the energy density. Poly(vinylidene fluoride) (PVDF) is the most widely used binder in commercial LIBs because of its high chemical resistance and excellent thermal and electrochemical stability.[25] As previously discussed, compared to the use of carbon black, the introduction of CNTs as conductive additives can greatly improve the gravimetric energy density (ca. ∼15%) of pouch cells; further, the CNTs are present at below 2 wt % and still maintain electrode integrity.[21−24] Therefore, most of the battery manufacturers have substituted CNTs for conventional carbon black. When applying CNTs to LIBs, a predispersed CNT solution is used to produce a homogeneous slurry and electrode.[26] Generally, the CNT solution includes a dispersant or surfactants to prevent self-aggregation of the CNTs, improve the electrode flexibility, enhance the solvation of the CNTs, and achieve suitable fluidic properties for enhancement of the dispersion stability.[27,28] Various surfactants and dispersants, including polyvinylpyrrolidone (PVP), nitrile butadiene rubber (NBR), cetrimonium bromide (CTAB), and other π-conjugated moiety-linked amphiphatic molecules, have been used to improve the dispersion of CNTs in fluids.[29−32] Hydrogenated NBR (HNBR), including a few unsaturated bonds (<5%), is known to improve not only the dispersion of CNTs but also the mechanical, chemical, physical, and thermal properties of the composite.[33] Owing to those functionalities, HNBR is often selected as a candidate for electrode materials to enhance flexibility; it is also used for polymer electrolytes or binders to maintain chemical and mechanical stability of composite networks. The use of HNBR, which is known to be easily deformable (up to 400%) under tensile stress lower than 2 MPa, leads to HNBR-based electrodes having a strength (0.6 N/cm) three times higher than that of PVDF-based electrodes (0.2 N/cm).[33−35] These characteristics are manifested in HNBR-containing electrodes and enable enhancement of the electrode flexibility. However, HNBR is not typically compatible with PVDF; HNBR results in inhomogeneous mixing of the PVDF slurry when present in a high concentration.[36] The poor uniformity and local aggregation of the slurry may result in poor electrical and mechanical behavior of the electrode and thus remain critical challenges. Moreover, from the viewpoint of increasing the electrode flexibility, a more facile methodology for homogeneous mixing and a high HNBR content should be developed to enable the fabrication of flexible electrodes for cylindrical cells. Electrode additive-driven improvement of slurry homogeneity involving both of PVDF and HNBR as electrode materials is a way to increase the electrochemical performance of cylindrical LIBs through production of flexible electrodes applied at their core. Among the reported studies on electrode additives for LIBs, studies about slurry homogeneity-derived inactive materials layers and their electrode flexibilities are not published (Table S2).

Here, we report that high-energy-density electrodes with high flexibility for use in cylindrical cells can be realized by introducing multifunctional additives. These additives overcome the inhomogeneous mixing of the slurry, enhancing the compatibility between the binder and HNBR in the CNT solution. Moreover, we show that a uniform CNT/binder network can be prepared by introducing such multifunctional additives. This homogenous CNT/binder network improves not only contact with active materials but also the mechanical properties of the electrodes. To prove the multifunctionality of the proposed additives, we applied them to two types of electrodes, relatively conductive additive/binder-rich free-standing electrodes and high-energy-density (active material loading of >98.4%) electrodes. We also discuss the origins of the additive-mediated electrochemical properties of the half-cells applied to the high-energy-density compositions. Our findings suggest that this facile and simple strategy based on multifunctional additives is effective for the realization of practical high-energy-density cylindrical cells.

EXPERIMENTAL SECTION

Materials Characterization. PVDF solution and CNT dispersion solution were purchased from Kureha Co., Ltd. (Japan) and Advanced Nano Products Co., Ltd. (Korea), respectively. Poly(melamine-*co*-formaldehyde) copolymer solution was purchased from Sigma-Aldrich. NMP was purchased from Daejung Chemical & Materials Co., Ltd. (Korea). $LiCoO_2$ (Montari Co., Ltd.) was used as received without further processing. The electrolyte was purchased from Welcos Co., Ltd. All reagents were used without further purification.

The rheological properties were measured using an Anton Paar Physica MCR 302 rheometer. The shear viscosity (shear rate of 1−500 s^{-1}) of the slurry was determined using a parallel plate with a 25 mm diameter and a 0.25 mm gap. Frequency sweeps were performed at room temperature with decreasing frequency from 100 to 0.1 rad/s and a strain of 1%. Proton NMR spectra of the PVDF/MF copolymers, except for the LCO and CNT mixture solutions with DMSO-d_6 as a solvent, were obtained using a Bruker DRX 300 spectrophotometer. Time-dependent NMR experiments were performed by collecting samples after high-shear mixing at 5000 rpm for various mixing times. To confirm the size of the CNTs with and without the MF copolymers, DLS measurements (NANO ZS, Malvern, Westborough, MA, USA) were performed at 25 °C. SAXS

https://doi.org/10.1021/acsami.1c00848
ACS Appl. Mater. Interfaces 2021, 13, 19970−19982

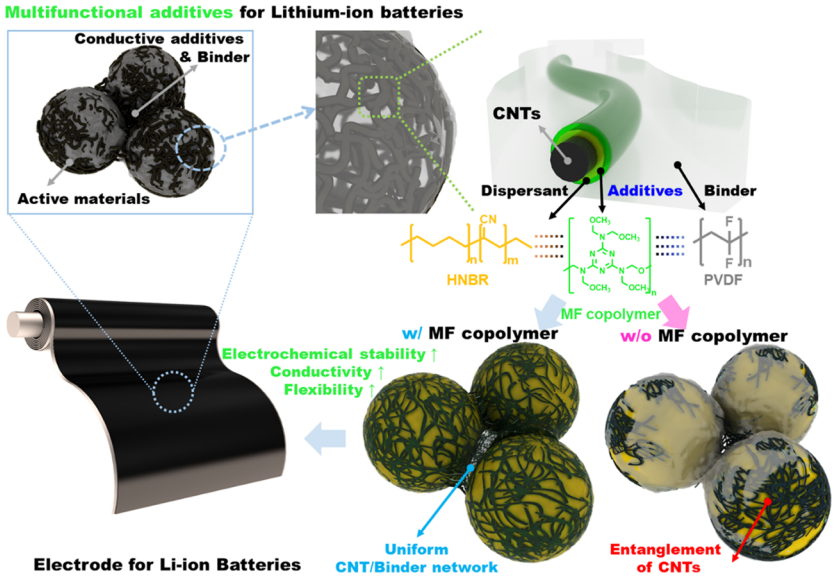

Figure 1. Illustration of multifunctional-additive-driven network improvement for LIB electrodes.

analysis of the LCO-free mixture solutions was performed using a NANOPIX (Rigaku) with a q range from 0.0218 to 40.16 nm. A Theta Probe AR-XPS system (Busan Center, KBSI, Korea) with ultrahigh vacuum chambers was used to obtain XPS data for the freestanding electrodes. The mechanical properties of the freestanding electrodes were measured using a dynamic mechanical analyzer (DMA Q800, TA Instruments) in tensile mode (0.1 N/min, preload at 0.02 N). The electrical conductivities of the freestanding electrodes were determined using probe-type resistance meters. Cu tape was attached to a slide glass with a constant gap (2 cm), and the freestanding electrodes were placed on Cu tape and fixed with silver paste. SEM images were obtained using a JSM-6700F (JEOL) under an accelerating voltage of 15 kV.

Fabrication of Electrodes and Electrochemical Characterization. The freestanding electrodes were fabricated by doctor-blade casting of slurry. Slurries were prepared by mixing specified ratios of $LiCoO_2$, CNT solution, and PVDF solution with or without MF copolymers at 4000 rpm for 15 min. The doctor-blade-coated films were first dried at 30 °C for 1 h in vacuum, and they were subsequently dried at 120 °C for 12 h in vacuum. The slurries for the high-energy-density electrodes were prepared by simple mixing of $LiCoO_2$, CNT solution, and PVDF solution at designated ratios at 4000 rpm for 15 min. The electrode layer was coated on Al foil (Welcos Co., Ltd.) using a doctor blade. The electrode was first dried at 80 °C for 1 h, and it was subsequently dried at 120 °C for 12 h in vacuum. The mass loadings of the electrode layers were approximately 7 or 16.5 mg/cm^2. The resistances of the high-energy-density electrode (4 cm^2) were measured using a Hioki electrode resistance meter (XF-057) with constant current (10 mA) and Al foil (resistance of 2.65×10^{-6} Ω cm^{-1}, thickness of 20 μm). To evaluate the electrochemical performance of the electrodes, coin cells (2032 coin half-cells) were assembled in a glovebox under highly pure Ar. A cell consisting of a Li counter electrode, a PP separator (Celgard 2400), and electrolyte solution (1 M $LiPF_6$ in EC/DMC (ethylene carbonate/dimethylcarbonate), 1:1 by volume) was assembled. The area of punched electrodes for cell assembly was 1.538 cm^2. Galvanostatic charge/discharge tests in the voltage range of 3−4.5 V at 25 °C were performed at various C rates (C/3, C/2, 1C, 2C, 3C, 4C, and 5C, where 1C corresponds to 150 mA g^{-1}) for $LiCoO_2$. Charge−discharge curves were recorded using a WBCS 3000 battery tester system (WonATech). Using a ZIVE SP1 electrochemical workstation (WonATech), electrochemical impedance spectroscopic analysis was performed at frequencies of 0.1 MHz to 0.1 Hz with a voltage amplitude of 0.01 V. The values of the resistances from cells are recorded in a semicircle from circular fitting of Nyquist plots. In addition, CV measurements were performed using half-cells in the voltage range of 3−4.5 V at a scan rate of 0.2 mV s^{-1}; the CNT/HNBR/PVDF film as a working electrode with a Li metal as a counter electrode was measured. A galvanostatic intermittent titration technique (GITT) of fresh cells was carried out at 0.1C and a current pulse time of 10 min.

RESULTS AND DISCUSSION

The effects of the melamine-formaldehyde (methylated) copolymers (MF copolymers) as functional additives for cylindrical LIBs are illustrated in Figure 1. PVDF solutions in *N*-methyl-2-pyrrolidone (NMP) and well-dispersed high-content conductive additive (CNT) solutions in NMP were used to achieve a homogeneous slurry, preventing agglomeration. Dispersing additives such as hydrogenated acrylonitrile butadiene rubber (HNBR), which individualize the CNTs and improve the electrode elasticity, were applied in this study before slurry mixing. In general, the mechanical flexibility of the electrodes is mainly dependent on the HNBR content in the slurry; however, the HNBR content must be limited because of the resulting gel-like aggregation.[33−36] This limitation mainly originates from the incompatibility of HNBR and PVDF, which leads to their self-aggregation. In the current work, during the slurry-mixing process, we offset the incompatibility by introducing MF copolymers containing active materials to the mixture solutions of CNTs, PVDF, and HNBR. The MF copolymer consists of 1,3,5-triazine, a flexible third amine and ether groups frequently used as an additive of separators, a N-doping reagent of active materials, and a cross-linker for mechanical maintenance of the composites.[37−40] For LIB applications, the thermal stabilities and cross-linking properties of MF copolymers are advantageous for preventing the elution of active materials and slurry inhomogeneity. Moreover, the 1,3,5-triazine backbones in the MF copolymer enable intensive interaction with CNTs, effectively restricting CNT folding.[41,42] Owing to the increased surface area of the well-dispersed CNTs that results from the inclusion of MF copolymers, HNBR-mediated gelation is restricted because of the loosened cross-linking of HNBR. In addition, the MF copolymer-mediated individualization of the CNTs affects their slurry dispersion during the general mixing process of the

https://doi.org/10.1021/acsami.1c00848
ACS Appl. Mater. Interfaces 2021, 13, 19970−19982

Table 1. Slurry Composition of High-Energy-Density and Freestanding Electrodes

Sample Name	Composition of slurry and electrode (wt%) Active Materials	Conductive additives	Binder	Dispersants	Additives	Total	Solid contents of Slurry	Electrode type	Ratio of Binder to Dispersants
	$LiCoO_2$	CNT (C)	PVDF (B)	HNBr (N)	Melamine (M)				
C04B10N008	98.52	0.4	1.0	0.08	-	100	78.59	Electrode on Foil	12.5
C04B10N008M008	98.44	0.4	1.0	0.08	0.08	100	78.64	Electrode on Foil	
C30B70N06	89.4	3.0	7.0	0.6	-	100	42.21	Freestanding electrode	11.66
C30B70N06M10	88.4	3.0	7.0	0.6	1.0	100	42.18	Freestanding electrode	
C50B70N10	87	5.0	7.0	1.0	-	100	36.43	Freestanding electrode	7.0
C50B70N10M10	86	5.0	7.0	1.0	1.0	100	36.40	Freestanding electrode	

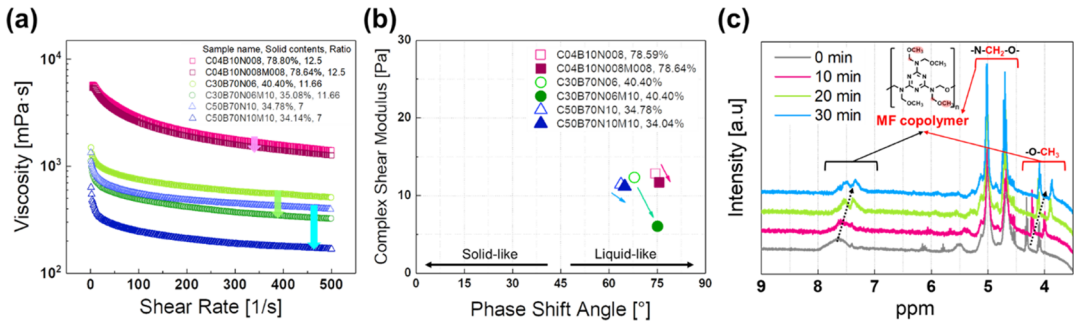

Figure 2. Characterizations of rheological properties of slurry with and without the MF copolymer. (a) Shear viscosity as a function of the shear rate of slurry. (b) Phase angle and complex shear modulus of slurry. The phase angle was calculated using recorded values (storage modulus G', loss modulus G'') at an angular frequency ω = 7.2 rad/s. (c) ^{1}H NMR spectra of mixture solution of the MF copolymer and PVDF in DMSO-d_6 after high-shear mixing for 0 (as soon as mixing), 10, 20, and 30 min.

active materials, conductive carbon, the binder, and the melamine additive. We analyzed the MF copolymer-mediated enhancements of the quality of the slurry, electrodes, and cells to demonstrate its suitability as an additive for electrodes placed at the cores of cylindrical cells.

Two types of electrodes were prepared: high-energy-density electrodes for practical cylindrical cells and freestanding electrodes without collectors; their slurry compositions are shown in Table 1. Because there is only 1.4 wt % CNT/PVDF networks in the high-energy-density electrodes, it is hard to discern the effects of functional additives (~0.08 wt %), such as physical and chemical properties of the slurry and electrode, and not proper for evaluating the flexibilities of electrode layers in the presence of Al collectors. Thus, freestanding model electrodes were used to examine the effects of MF copolymers (1 wt %) containing excess amounts (10−12 wt %) of CNT/PVDF networks in electrodes.

Rheological analysis was performed to evaluate the quality of the coated layer during film formation with a shear force applied to the slurry, as shown in Figure 2. The shear viscosity and viscoelasticity of the slurry were confirmed (Figure 2a,b). To the best of our knowledge, the remarkable shear-thinning effects at the same composition result in improved qualities of coating layers on collectors.[43] The viscosities decreased when the MF copolymers were introduced into the slurry. In addition, upon increasing the CNT content from 3 to 5% for the slurry for C30B70N08M10 (vs C30B70N08) and C50B70N10M10 (vs C50B70N10), the degree of the viscosity decrease increased. Furthermore, in the analysis of the viscoelastic behavior, an MF copolymer-induced shift of the phase angle was observed, implying enhancement of the liquid-like properties of the slurry. These phenomena indicate that the limitations originating from the increase in the HNBR content in the slurry and increased electrode flexibility were overcome by the addition of MF copolymers.

The origins of the changes of the slurry properties upon introduction of MF copolymers were investigated using a mixture of electrode materials in the absence of active materials. To confirm the effects of the MF copolymers on the CNT/PVDF networks without active materials, we analyzed the solution-state properties of CNT/PVDF with and without MF copolymers. With MF copolymers on the CNTs, the average size distribution shifted to a smaller range, with a sharpened peak compared with those of pristine CNTs,

https://doi.org/10.1021/acsami.1c00848
ACS Appl. Mater. Interfaces 2021, 13, 19970−19982

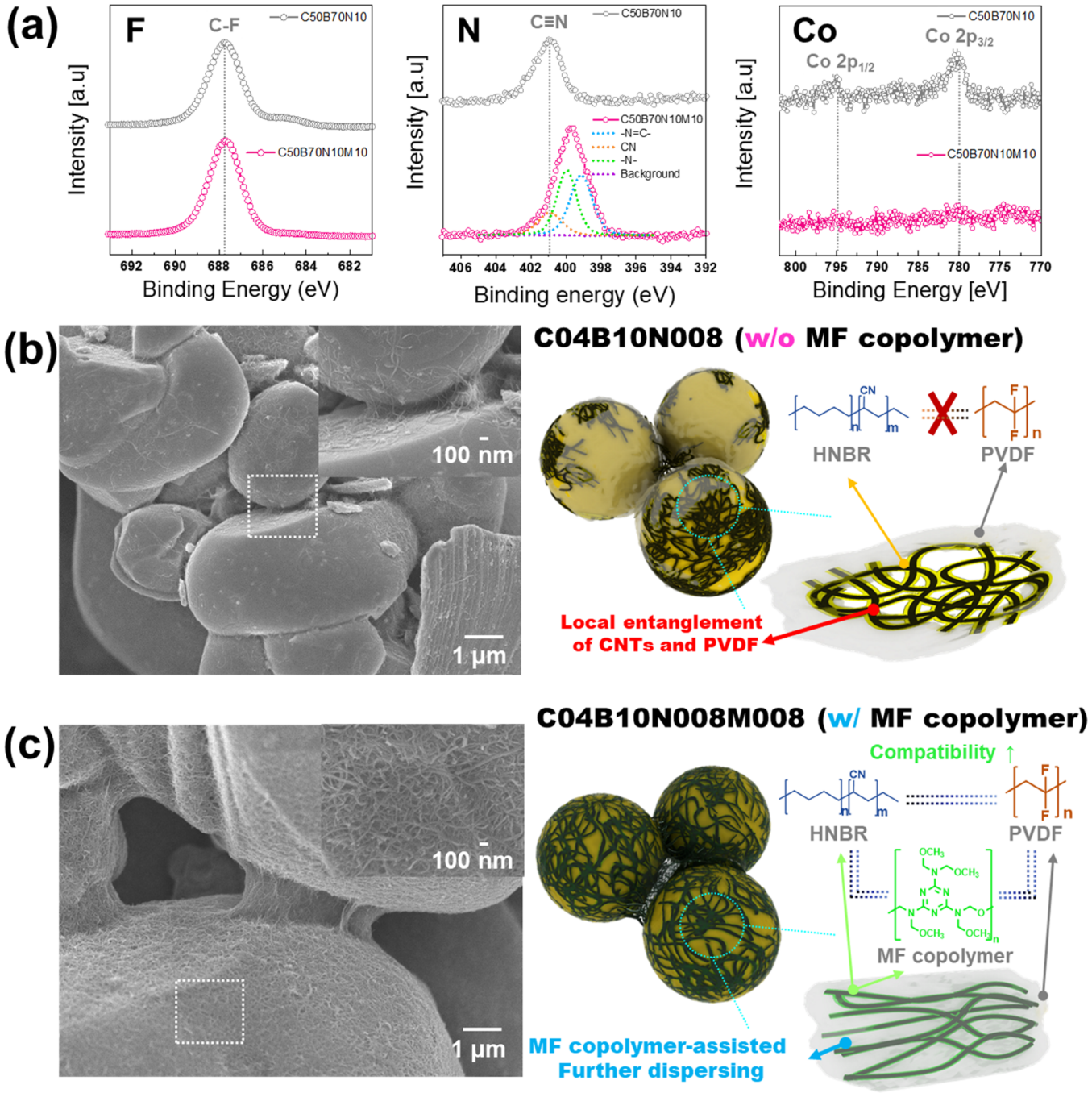

Figure 3. Characterizations of the surface structure of electrodes. (a) XPS spectra of C50B70N10 and C50B70N10M10 and SEM images corresponding to schematic illustrations of (b) C04B10N008 and (c) C04B10N008M008 showing MF copolymer-induced improvement of CNT/PVDF networks wrapped on active materials.

indicating improved monodispersity (Figure S1). The physical interaction of π electrons between the aromatic carbon of the CNTs and the 1,3,5-triazine backbone of the MF copolymers may create barriers prohibiting agglomeration of CNTs as well as bridge materials, leading to enhanced affinity with NMP *via* formation of CNT/MF copolymer composites.[32] Because physical interactions of certain components of the mixture (PVDF) with MF copolymers may have occurred, molecular-level analysis was performed using NMR spectroscopy, with results shown in Figure S2 and Figure 2c. Time-dependent ^{1}H NMR monitoring of the mixture (PVDF with MF copolymers in the absence of LCO) at 5000 rpm was performed. NMR spectroscopy was used to clarify monomer peaks or peaks from physically cross-linked dimer or trimer molecules.[44] As can be seen in Figure 2c, the NMR spectra of the polymer blends in the range of 3.5−9 ppm revealed the coexistence of highly self-aggregated MF copolymer species (~7.5 ppm) and relatively isolated MF copolymer species (3.5−5 ppm) at room temperature.[45] Changes of the peak shape, as well as chemical shifts, were observed for the melamine backbone (~7.5 ppm) and terminal $-OCH_3$ groups of the MF copolymers in time-dependent NMR spectra of the PVDF/MF copolymer blends.[45−47] This chemical shift is related to inter- or intrapolymer interactions originating from the dipole−dipole

https://doi.org/10.1021/acsami.1c00848
ACS Appl. Mater. Interfaces 2021, 13, 19970−19982

interaction of protons adjacent to 1,3,5-triazine moieties as well as protons in the alkyl chain (involving ether) of the MF copolymers.[46,47] However, no peak shift of PVDF as a function of mixing time was observed (Figure S2).[48] Figure S2 confirms the absence of interaction between the MF copolymers and PVDF; it is also possible that there was weak interaction that was not sufficient for peak shifts of PVDF to be evident. The mixture solutions comprising MF copolymers and HNBR in DMSO also produced physical interactions, as shown in the ^{1}H NMR spectra (Figure S3). Pristine HNBR showed peaks at around 2.95 and 1.2 ppm, corresponding to a proton adjacent nitrile group and alkyl chain repeating units of the hydrogenated part, respectively.[49,50] Upon addition of MF copolymers during high-shear mixing, the peak at 2.95 ppm originated from protons adjacent to CN functional groups are almost the same with that after 20 min (2.94 ppm). One peak from the alkyl chains (1.19 ppm) may also have shifted and overlapped with a butanol peak at approximately 1.21 ppm during mixing. These NMR results suggest that MF copolymers that interact with HNBR are not enough to form relatively individualized compounds under diluted systems (ca. 2 wt %). However, their weak interaction may act as more critical factors for HNBR compatibility under high-shear mixing in the slurry due to the relatively higher solid contents of approximately 78 wt %. The DLS and NMR results indicate that physical rearrangement of MF copolymers during high-shear mixing led to an enhancement of the monodispersity of the CNTs, as well as to modification of the CNT/PVDF properties. Mixture solutions of CNT/HNBR and PVDF with and without MF copolymers excluding LCO powder were prepared by a high-shear mixing process, and their rheological behavior was analyzed (Figure S4). Mixture solutions (excluding LCO powder) showed similar rheological properties in Figure 2a,b. XRD patterns of CNT/HNBR/PVDF films with and without MF copolymers excluding LCO powder are shown in Figure S5. The peak at around 11.7° in the XRD pattern is associated with the (001) interlayer structure of CNTs. The peaks at 18.4, 19.8, and 25.5° correspond to 020, 110, and 021 reflections, respectively, of the monoclinic α-phase crystal of PVDF.[51] The peak at 25.5° may be the sum of the 021 reflection of raw PVDF powder of the α-phase crystal and the 002 reflection of CNTs (JSPDS no. 96-101-1601).[51] Upon addition of MF copolymers during composite formation, shifts of the peak of approximately 20 and 35° were found in the XRD pattern. The peaks at 20.2° (110/200 reflection) and 36.3°, related with the β-phase crystal of PVDF, are shown in Figure S5.[51,52] The enhancement of the β content in the composite films with the MF copolymer, compared to that in the CNT/PVDF/HNBR mixture, implies that interactions of the MF copolymer with components in the composites influenced the PVDF crystal structure. Relatively higher β-phase contents in PVDF are known to be a factor that enhances the electrochemical performance of Li-ion batteries.[53] MF copolymer-induced conformation tuning of PVDF may lead to the achievement of an optimized CNT/PVDF/HNBR structure application to Li-ion batteries. Cyclic voltammetry (CV) measurements in 1 M $LiPF_6$ EC/DMC (1:1) solutions in the voltage range of 3−4.5 V were also performed for the LCO-free CNT/HNBR/PVDF film with and without MF copolymers. In Figure S6, no oxidation/reduction peaks are observed, and the integrated curve area of the sample with MF copolymers is larger than that of the sample without MF copolymers. The increase in the area is caused by the change of the surface area of the CNT/PVDF network incorporating MF copolymers.

X-ray photoelectron spectroscopy (XPS) analysis of the film-coated freestanding compositions (C50B70N10 and C50B70N10M10) was performed (Figure 3a and Figure S7). The shoulder peak of F 1s in C50B70N10, derived from PVDF adjacent to the LCO crystal, is at approximately 685.08 eV, providing evidence of direct contact between PVDF and LCO; this peak vanished in the presence of MF copolymers (C50B70N10M10). In addition, the presence of a peak originating from the lattice oxygen at ∼529 eV for C50B70N10 was evidence of exposed LCO surfaces, while this peak was not observed for C50B70N10M10, with full coverage of LCO surfaces *via* CNT/PVDF/MF copolymer networks (Figure S7). The change of the F 1s peak with the addition of MF copolymers suggests enhancement of contact between CNTs and active materials. With the presence of MF copolymers in the electrodes, peaks from 1,3,5-triazine (399.18 eV) and the third amine (399.98 eV) in the MF copolymers were observed for the N 1s spectra.[54] After the introduction of MF copolymers (C50B70N10M10), the Co 2p peaks (780.08 and 795.18 eV) observed for C50B70N10 vanished, indicating that more uniform CNT/PVDF networks (resulting from the addition of MF copolymers) wrapped the active materials. The C 1s peaks mainly corresponded to PVDF (C−F at 290.88 eV) and CNTs (C═C at 284.58 eV).[55,56] We analyzed the ratio of the peak areas of C−F (PVDF) to C═C (CNTs) to confirm the MF copolymer-mediated changes of the surface structures of the electrodes. Because of the differences in hydrophobicity, the peak area of C═C in C50B70N10 was 10 times larger than that of C−F despite the electrode containing 5% MWCNTs and 7% PVDF. A decrease was observed in the C═C/C−F area ratio of the electrodes with MF copolymers compared with that of the electrodes without MF copolymers. These results indicate that the CNT content (indirect contact with LCO) on the electrode surface decreased with addition of MF copolymers. In other words, local aggregation of CNT/PVDF networks originating from differences in hydrophobicity was offset by interaction of CNT-MF copolymers. The MF copolymer-mediated CNT/PVDF network changes were confirmed by small-angle X-ray scattering (SAXS) analysis. The weak nanoscale regularity induced by PVDF vanished upon addition of MF copolymers (Figure S8). This result indicates the collapse of the subnanoscale crystallinity. The MF copolymer-derived network homogeneity in the high-energy-density compositions (C04B10N008 and C04B10N008M008) is also confirmed in Figure 3cb,. SEM images of C04B10N008M008 reveal relatively well-dispersed and conserved CNT/PVDF networks compared with those in C04B10N008. These findings suggest that the MF copolymer-derived network homogeneity was intensified. In Figure 3b,c, the slurry networks formed with and without addition of MF copolymers are presented for comparison. The MF copolymer (1) acts as an adhesive between the active materials wrapped with the CNT/PVDF network and (2) prevents the self-assembly of CNTs and the formation of PVDF nanocrystals in the slurry networks.

To confirm the effects of MF copolymers on CNT/PVDF-rich compositions, freestanding electrodes, without collectors, were prepared using blade casting. A summary of the freestanding electrodes with compositions C30B70N06, C30B70N06M10, C50B70N10, and C50B70N10M10 is presented in Table S1. Improvements of the conductivities of

https://doi.org/10.1021/acsami.1c00848
ACS Appl. Mater. Interfaces 2021, 13, 19970−19982

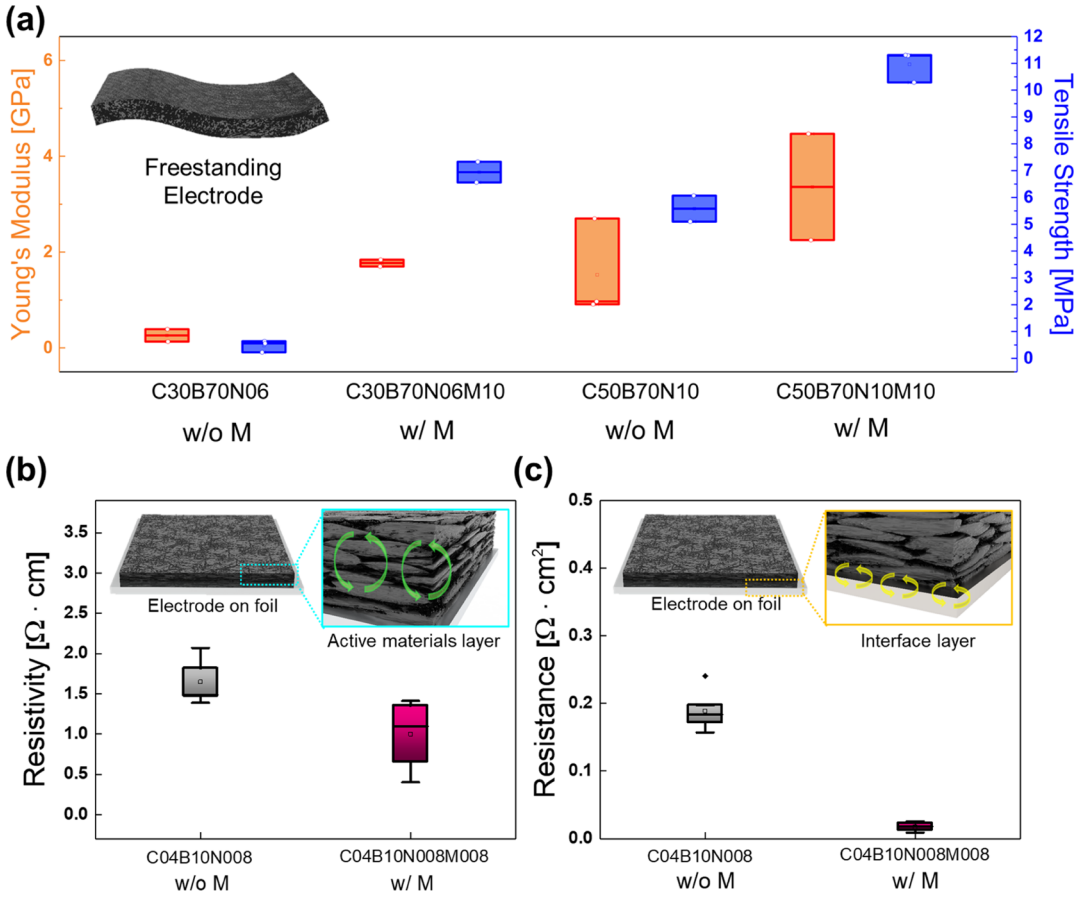

Figure 4. Mechanical and electrical properties of electrodes. (a) Mechanical properties of freestanding electrodes (C30B70N06, C30B70N06M10, C50B70N10, and C50B70N10M10). (b) Resistivity of the active material layer of high-energy-density electrodes (C04B10N008 and C04B10N008M008). (c) Resistance of the interface layer of high-energy-density electrodes (C04B10N008 and C04B10N008M008). Pressed electrodes were used for (b) and (c).

the freestanding electrodes in the presence of MF copolymers were observed for C50B70N10 (2.94 S/cm) and C50B70N10M10 (6.65 S/cm). The SEM images of the freestanding electrodes in Figure S9 reveal well-aligned morphologies and CNT/PVDF networks wrapping the active materials. Dynamic mechanical analysis (DMA) measurements were performed, with results shown in Figure 4a. Increasing the CNT content in the slurry from 3 to 5% resulted in enhancement of the tensile strength and Young's modulus of the freestanding electrodes. In addition, the mechanical properties of the freestanding electrodes containing MF copolymers (C30B70N06M10 and C50B70N10M10) were approximately 4 and 2 times higher, respectively, than those of the pristine electrodes. This enhancement originated from the formation of a uniform slurry, which was achieved by restraining the self-aggregation of CNTs and PVDF and enhancing contact between CNTs and LCO.

Fundamental analysis of the resistance of individual electrodes for high-energy-density electrodes was performed using an electrode resistance meter (Hioki, XF-057).[57,58] With the addition of the MF copolymer (constant binder content), the resistivity of the electrode layer and the interface resistance decreased from 1.52 to 1.0 Ω/cm and from 0.038 to 0.017 Ω/cm^2, respectively, after pressing, indicating that the adhesive properties of the CNTs were enhanced due to physical interaction with MF copolymers (Figure 4b,c). The improvement in the interface resistance was caused by interaction between lone-pair electrons (oxygen or nitrogen atoms in the MF copolymer) and metal atoms on the collector.[59] Direct evidence of MF copolymer-mediated improvement of the electrical properties was observed through evaluation of CNT/PVDF networks with high-energy-density compositions at the electrode level. Owing to the MF copolymer-assisted network modifications of the electrodes, high-energy-density electrodes containing 1.56% additives were successfully fabricated. Upon increasing the MF copolymer content in the slurry, a trade-off point of 0.08% was confirmed, with excess MF copolymers not interacting with the CNTs; this noninteraction may act as an offset factor, limiting conductance of the electrodes (Figure S10).

To date, the utilization of electrodes in the cores of cylindrical cells has been restricted because of the lack of flexibility of the electrode layers. Although researchers have worked to increase the electrode flexibility, lack of fluidic behavior of the slurry and local aggregation after slurry fabrication are observed upon an increase in the additive content (binders and conductive additives). As previously discussed, the decrease in resistivity of the active materials layer, and interface resistance occurring with introduction of MF copolymers in electrodes, implies that the quality of electrodes at the cores of cylindrical cells may be higher than that of MF copolymer-free electrodes. To indirectly compare the quality of electrodes at the cores of cells, electrodes were rolled onto cylinder substrates with core diameters of 1 and 10

https://doi.org/10.1021/acsami.1c00848
ACS Appl. Mater. Interfaces 2021, 13, 19970−19982

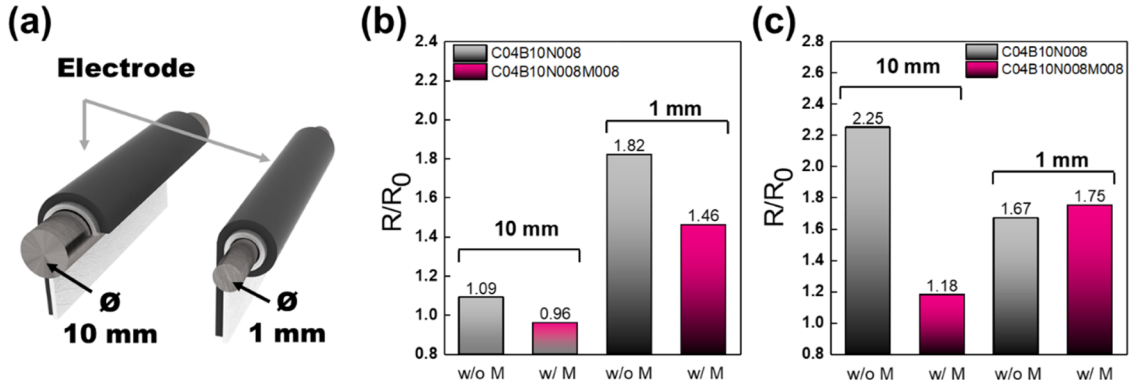

Figure 5. Flexibilities of high-energy-density electrodes. (a) Illustration of sample preparations to examine electrode flexibility. (b) Degree of the resistivity increase of the active material layer and (c) resistance increase of the interface layer after the electrode was rolled with cylindrical substrates (10 or 1 mm) for C04B10N008 and C04B10N008M008 (R_0 is the value before rolling with cylindrical substrates, and R is the value after rolling with cylindrical substrates).

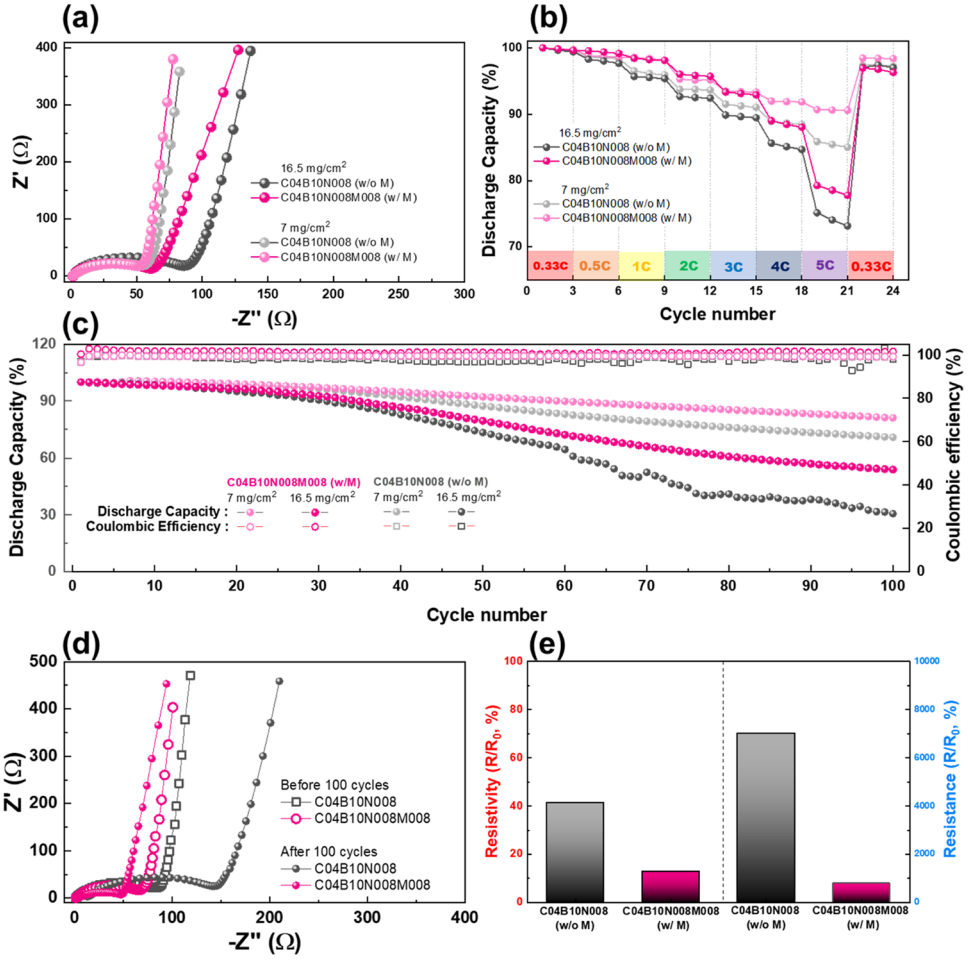

Figure 6. Electrochemical properties of high-energy-density LIBs. (a) Nyquist plots, (b) rate capability tests (0.33C−5C), and (c) cycling performance (at 0.33C) of high-energy-density C04B10N008 (7 and 16.5 mg/cm^2) and C04B10N008M008 (7 and 16.5 mg/cm^2), (d) EIS profiles of cells before and after 100 cycles (16.5 mg/cm^2), and (e) degree of resistance changes of electrodes before and after 100 cycles collected by cells with DMC and ethanol washing (16.5 mg/cm^2), area of the electrode in cells: 1.538 cm^2.

mm (Figure 5a), and the resistivity of the active layer and the interface resistances were measured. Changes of resistance before and after rolling of electrodes onto cylinder substrates are shown in Figure 5b,c. Resistivity of electrode active layers both with and without MF copolymers increased; however, the degree of the resistivity increase of the electrodes with MF copolymers (~96% at 10 mm and 146% at 1 mm) was lower than that of the electrodes without MF copolymers (109% at 10 mm and 182% at 1 mm). That is, electrodes containing MF copolymers were more flexible than electrodes without them. The increase in the interface resistance in C04B10N008M008 rolled on a 10 mm substrate was lower than that for C04B10N008; however, similar levels of the resistance increase were achieved when the electrodes were rolled onto a 1 mm

https://doi.org/10.1021/acsami.1c00848
ACS Appl. Mater. Interfaces 2021, 13, 19970−19982

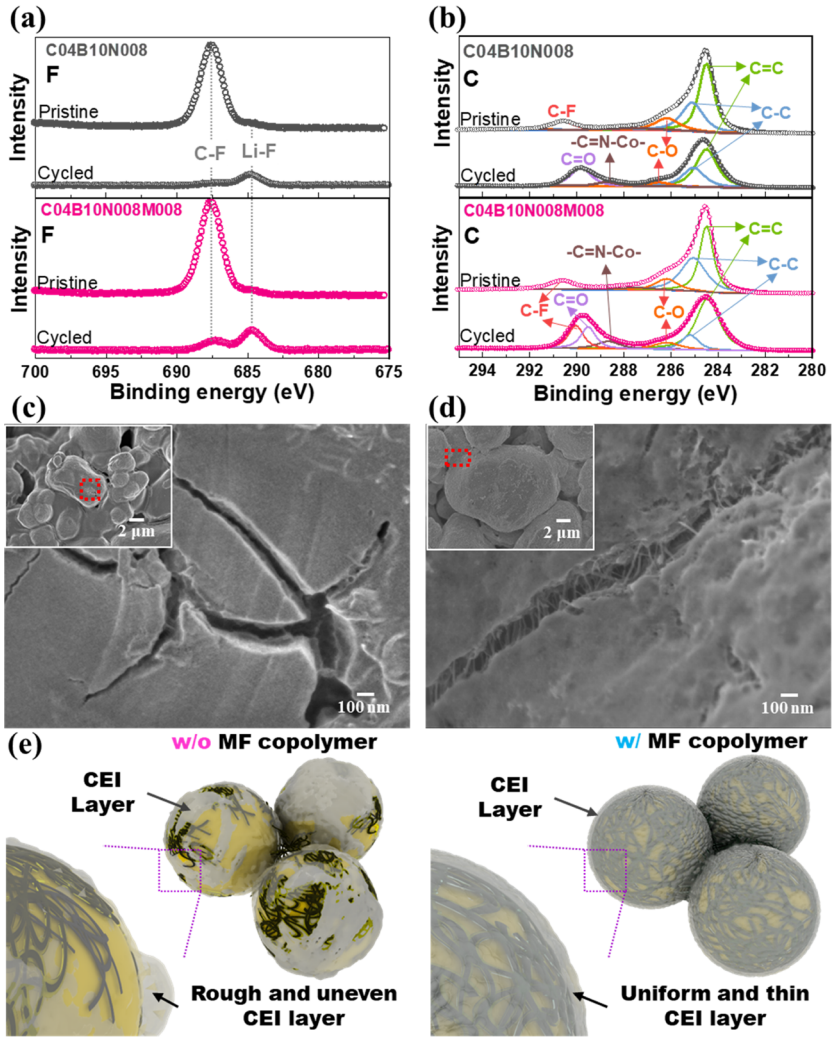

Figure 7. Interfacial study of cycled electrodes. XPS spectra of fresh and 100-cycled electrodes: (a) F 1s and (b) C 1s spectra and SEM images of (c) cycled C04B10N008 and (d) cycled C04B10N008M008. (e) Schematic presentations of CEI layers of cycled C04B10N008 and C04B10N008M008.

substrate. In addition, because of cross-linking between MF copolymers, contact resistance in the active layer between the cracked area in the presence of MF copolymers was lower than that of pristine electrodes. Contact between the collector and the active layer with MF copolymers after electrodes were rolled onto a 10 mm substrate was maintained; however, contact weakened after electrodes were rolled onto a 1 mm substrate because of the activation energy needed for reformation of bonding between MF copolymers and collectors.

Thick electrodes with maximized active material loading (>98%) and mass loading (>16 mg/cm^2) are needed; information on the electrochemical performance of thick electrodes can be directly used as basic data to improve the performance of Li-ion batteries. Thus, two types of high-energy-density electrodes with different mass loadings of ∼7 and ∼16.5 mg/cm^2, and a constant CNT/binder ratio (0.4/1.0 wt %), were prepared to evaluate the effect of MF copolymers. Half-cells with C04B10N008 or C04B10N008M008 were used to confirm the electrochemical properties. Electrochemical impedance spectroscopy (EIS) results are presented as Nyquist plots in Figure 6a. Impedance from the charge-transfer process (R_{ct}) of C04B10N008M008 (67.2 Ω for 16.5 mg/cm^2 and 54.5 Ω for 7 mg/cm^2) was smaller than that for the MF copolymer-free cells (93.1 Ω for 16.5 mg/cm^2 and 59.4 for 7 mg/cm^2). In addition, the slope of the straight line in the low-frequency range indicates that the Li-ion diffusion of C04B10N008 was similar to that of C04B10N008M008, at 7 mg/cm^2. However, the slopes of C04B10N008 were relatively steeper than those of C04B10N008M008 at a high level of mass loading (16.5 mg/cm^2). The galvanostatic intermittent titration technique (GITT) was employed to compare quantitative values of Li-ion diffusion coefficients in the first free cycles in a 0.1C voltage range from 3 to 4.5 V; results are shown in Figure S11a. The inset graph indicates voltage changes before and after current pulse during charging. The value of $(\Delta E_s/\Delta E_t)^2$, which is the voltage change at specific times during charging for C04B10N008, increased from 0.96 to 1.04 due to the weakened coverage capability of the CNT/PVDF network during cycling, as can be seen in the Figure S11c. That value of C04B10N008M008 decreased from 1.3 to 0.88, indicating that the MF copolymer improved the coverage capability of the CNT/PVDF networks at relatively higher mass loading (Figure S11c). Values of Li-ion diffusion coefficients of C04B10N008 of 1.03 × 10^{-8} (7 mg/cm^2) and 5.54 × 10^{-8} (16.5 mg/cm^2), as well as those of C04B10N008M008 of 1.48

https://doi.org/10.1021/acsami.1c00848
ACS Appl. Mater. Interfaces 2021, 13, 19970−19982

$\times 10^{-8}$ (7 mg/cm^2) and 3.8 $\times 10^{-8}$ (16.5 mg/cm^2), correspond to the tendencies of the slopes of the straight lines in Figure 6a (Figure S11b). This behavior may originate from MF copolymer-induced stable preservation of relatively well-wrapped CNT/PVDF networks on LCO in electrolytes.[60] The discharge capacities of C04B10N008 and C04B10N008M008 at different rates (0.33C−5C) were also determined. As shown in Figure S12, relatively higher discharge capacities at 5C were maintained for C04B10N008M008 than for C04B10N008 (163 mA h/g (7 mg/cm^2) and 139 mA h/g (16.5 mg/cm^2) vs 156 mA h/g (7 mg/cm^2) and 136 mA h/g (16.5 mg/cm^2), respectively). The rate capabilities calculated for 5C/0.33C were 85.4% (7 mg/cm^2) and 75% (16.5 mg/cm^2) for C04B10N008 and 90.6% (7 mg/cm^2) and 78.5% (16.5 mg/cm^2) for C04B10N008M008, indicating the relative stability of C04B10N008M008 compared with C04B10N008, despite the different mass loadings (Figure 6b). The stability over 100 cycles of LCO cathodes with MF copolymers was also compared with that of LCO cathodes without MF copolymers at 0.33C (Figure 6c). The charge−discharge curves obtained during cycling are shown in Figure S13. The voltage changes upon operation of C04B10N008 after free cycling are remarkably drastic compared to those of the C04B10N008M008 cells, though voltage changes derived by differences of mass loading are more critical for capacity fading. The discharge capacities of C04B10N008M008 after 100 cycles, 146.95 mA h/g (7 mg/cm^2) and 99.18 mA h/g (16.5 mg/cm^2), were higher than those of C04B10N008, 129.07 mA h/g (7 mg/cm^2) and 55.25 mA h/g (16.5 mg/cm^2) (Figure 6c). The degree of mass loading is a relatively crucial factor resulting in a decline of discharge capacity in high-energy-density (>98.4%) LIBs. The ratios of the discharge capacities of the 100th/1st cycle (%) were 81.14% (7 mg/cm^2) and 54% (16.5 mg/cm^2) for C04B10N008M008 and 71% (7 mg/cm^2) and 30.7% (16.5 mg/cm^2) for C04B10N008 (Figure 6c). Even at different mass loadings, the cells with MF copolymer-containing electrodes maintained higher capacity retentions after 100 cycles than the MF copolymer-free ones. Moreover, the MF copolymers, which tuned the electrical network, had a relatively greater effect on stable cell operation for the 16.5 mg/cm^2 mass loading. These results suggest the importance of well-wrapped CNT/PVDF tuned from MF copolymers, which prevents direct contact of the electrolyte and the surface of LCO, for stable charge−discharge cycling.[61] In addition, crystal structures of the 1,3,5-trazine backbone with cobalt ions are frequently reported, indicating that the MF copolymers contribute to enhanced CNT/PVDF wrapping of LCO during cycling.[62,63] Recently, Yang et al. reported the importance of coordination bonding formation between nitrile and LCO in the charging step.[63] Their findings imply that the MF copolymer-mediated contact enhancement between the HNBR-wrapped CNTs and LCO may result in the formation of additional chemical bonds between them during the charging step. To determine the reasons for the differences in the electrochemical performance resulting from the addition of MF copolymers, analysis of half-cells and their electrodes was performed before and after 100 cycles. EIS results for C04B10N008 and C04B10N008M008 at 16.5 mg/cm^2 before and after 100 cycles are presented in Figure 6d. Changes of amplitudes of semicircles (R_a) and x-axis intercepts (R_x) in Nyquist plots before and after 100 cycles are compared. After 100 cycles, values of ΔR_x and ΔR_a of the half-cells were 10.54 and 43.8 Ω, respectively, for C04B10N008, compared with 4.01 and −30.25 Ω, respectively, for C04B10N008M008. Enhancement of the R_a values during long charge−discharge cycling is a generally observed phenomenon.[64] However, a decrease in the R_a values after 100 cycles from 74.37 to 44.12 Ω was observed. To compare the resistances of the interface and the active layer of the pristine (R_0) and cycled electrodes (R) after DMC and ethanol washing, the R/R_0 (%) values of C04B10N008 and C04B10N008M008 are presented in Figure 6e. Significant increases of the interface and active layer resistances of C04B10N008 (ΔΩ of 7012% and ΔΩ of 41%) compared with those for C04B10N008M008 (ΔΩ of 775% and ΔΩ of 12%) were observed.

To explore the origins of the electrochemical performance enhancement, surface chemical compositions of cycled electrodes were determined using XPS analysis, as shown in Figure 7 and Figures S14 and S15. The F 1s spectra of the electrodes both before and after cycling contain C−F (687.68 eV) and Li−F (684.78 eV) peaks (Figure 7a). However, the C−F peak, an indicator of PVDF, of the cycled C04B10N008M008 is more prominent than that of the cycled C04B10N008. This result indicates that the CEI layers of the cycled C04B10N008M008 were relatively thin compared with those of the cycled C04B10N008 and that less side product was deposited on the electrode surfaces for the cycled C04B10N008M008. C 1s spectra were also obtained to compare the polycarbonate products in the CEI layers of both electrodes (Figure 7b). Because of the C−F peaks in the F 1s spectra of the cycled C04B10N008M008, the peak at 289.8 eV can be considered a combination of the C−F (290.05 eV) and C═O (289.52 eV) peaks. The peak shift of ∼0.6 eV of the C−F peak after cycling may be attributed to the thin CEI layers.[65] However, the intensity of the C−F peak in the F 1s spectra of the cycled C04B10N008 is very low compared with that of the cycled C04B10N008M008. Thus, the peak at 289.83 eV should originate from carbonate species. The amount of side products, determined from the ratio of the peak area of C═O (289.83 or 289.52 eV) to that of C═C (284.5 eV), involving the C═O groups in cycled C04B10N008, was relatively higher than that in cycled C04B10N008M008 (Figure 7b and Figure S14). This result indicates that the cycled C04B10N008M008 had a CEI layer thinner than that of the cycled C04B10N008. The N 1s spectra of C04B10N008 before and after cycling show slight differences caused by bond formation between N and Co, i.e., the −CN−Co− peak (398.03 eV) (Figure S15a).[63] A correlated peak for −CN−Co− was also observed at 288.6 eV in the C 1s spectra.[66] In addition, the nitrile peak (400.9 eV) vanished after 100 cycles in C04B10N008M008, and its disappearance was accompanied by the appearance of a −CN−Co− peak (398.08 eV), indicating that the MF copolymer boosts the formation of coordination bonds between lone-pair electrons of −CN and LCO during charge−discharge cycling.[63] The Co 2p spectra of the cycled electrodes reveal peak shifts to lower energy, from 780.18 to 778.08 eV and from 795.18 to 793.18 eV (Figure S15b). These shifts, resulting from the decrease in the Co oxidation state, imply that the N 2p orbital in the nitrile hybridizes with the Co 3d state of LCO to form Co−NC−R.[67] The complex formation between MF copolymers and Co ions, as mentioned above, may also contribute to stabilizing the LCO surfaces during cycling. The formation of thin and uniform CEI layers is important for stable operation in a high-voltage range, preserving the crystal structures of the active materials,

https://doi.org/10.1021/acsami.1c00848
ACS Appl. Mater. Interfaces 2021, 13, 19970−19982

suppressing the deposition of carbonate species, and conserving the electric networks.[63] The CNT/PVDF microstructures covered with cathode−electrolyte interface (CEI) layers after 100 cycles are shown in Figure 7c,d. The CEI layers deposited on CNT/PVDF are similarly shown for electrodes with and without MF copolymers (insets of Figure 7c,d). Morphological differences are observed by comparing cracks of the CEI layer, which expose the inner CNT/PVDF networks on the active materials. For C04B10N008, partially exposed active materials with severe cracks, as well as disconnected electric network structures between LCOs, are observed. Figure 7e shows the effects of the MF copolymers on the LCO cathode after 100 cycles. In contrast, relatively well-conserved networks can be observed in Figure 7e, suggesting the multifunctionality of the MF copolymer, including (1) contact enhancement between HNBR/CNT and LCO inducing coordination bonding formation under cycling and (2) chelating properties of the MF copolymer with LCO. Through protection of LCO *via* formation of composite layers tuned by MF copolymers, a relatively thin and stable CEI layer was formed, enabling the enhanced CNT/PVDF networks to be conserved during long-term charge−discharge cycling. The ripple effects of this work on electrode additives for cathodes of Li-ion batteries are obvious, i.e., only 0.08 wt % MF copolymer is capable of enhancing stability by ∼176% (Table S2).

CONCLUSIONS

In summary, we have demonstrated the use of MF copolymers as functional additives for the realization of high-energy-density cylindrical LIBs. The MF copolymers underwent rearrangement during mixing of a slurry containing CNTs, HNBR, PVDF, and LCO, producing a relatively more homogeneous slurry than that of the reference as well as increasing CNT dispersity and β-phase PVDF. Owing to the MF copolymer-mediated contact enhancement between the CNTs and LCO, the mechanical properties and conductivities of the freestanding electrodes were enhanced ∼2 times. The active-layer resistivity and interface resistances of high-energy-density electrodes containing MF copolymers were also enhanced by 34 and 55%, respectively, compared with those of the pristine reference, owing to interaction of the MF copolymers and metal collectors. Interestingly, the degree of the resistance increase of the electrodes after they were rolled onto cylinder substrates with diameters of 1 or 10 mm was relatively lower for the MF copolymer-containing electrodes than for the pristine electrodes. Furthermore, the well-formed CNT/PVDF/MF copolymer networks on LCO resulted in a more stable capacity retention of 81.14% (pristine: 71%) and a better rate capability of 90.6% (pristine: 85.4%) at 7 mg/cm^2, as well as a capacity retention of 54% (pristine: 30.7%) and a rate capability of 78.5% (pristine: 75%) at 16.5 mg/cm^2. After 100 cycles, the electrode containing MF copolymers possessed a relatively thin CEI layer with conserved CNT/PVDF networks. Chemical and physical bond formation between nitrile or cyclic triazine and LCO during the cycles was also enhanced by the MF copolymers, resulting in improved electrochemical performance. This characterization of cathodes containing MF copolymers suggests that important factors for achieving stable charging−discharging include meticulous wrapping of active materials for enhanced contact as well as the presence of chemical/physical bond formation during cycling and protection of the layer from electrolyte-derived highly reactive species. We believe that our findings on both the electrode and the cell level will contribute to improving the stability and energy density of cylindrical high-energy-density electrodes for LIBs.

ASSOCIATED CONTENT

Supporting Information

The Supporting Information is available free of charge at https://pubs.acs.org/doi/10.1021/acsami.1c00848.

Particle size distribution of CNTs and CNT/MF copolymers; ^{1}H NMR spectra of MF copolymers/PVDF and MF copolymers/HNBR; rheological analysis, WAXS patterns, and CV curves of LCO-free CNT/PVDF/HNBR films with or without MF copolymers; XPS spectra, SEM images, and summaries of freestanding electrodes; SAXS spectra of LCO-free CNT/PVDF films; resistivity of the active materials layer and the resistance interface layer of high-energy-density electrodes at various amounts of the MF copolymer; GITT results and raw charge−discharge curves of high-energy-density electrodes; XPS spectra of cycled electrodes with or without MF copolymers; comparison of our work with previously reported studies (PDF)

AUTHOR INFORMATION

Corresponding Authors

Jin Woo Yi − *Carbon Composites Department, Korea Institute of Materials Science (KIMS), Changwon 51508, Republic of Korea*; Email: yjw0628@kims.re.kr

Jung-Keun Yoo − *Carbon Composites Department, Korea Institute of Materials Science (KIMS), Changwon 51508, Republic of Korea*; orcid.org/0000-0002-9693-649X; Email: yoojk@kims.re.kr

Authors

Junho Ahn − *Carbon Composites Department, Korea Institute of Materials Science (KIMS), Changwon 51508, Republic of Korea*

Byeongho Park − *Carbon Composites Department, Korea Institute of Materials Science (KIMS), Changwon 51508, Republic of Korea*

Jongsoon Kim − *Department of Energy Science, Sungkyunkwan University, Suwon 440-746, Republic of Korea*

Moon-Kwang Um − *Carbon Composites Department, Korea Institute of Materials Science (KIMS), Changwon 51508, Republic of Korea*

Complete contact information is available at: https://pubs.acs.org/10.1021/acsami.1c00848

Author Contributions

All authors have given approval to the final version of the manuscript.

Notes

The authors declare no competing financial interest.

ACKNOWLEDGMENTS

This research was supported by Research Fund (PNK7330, PNK7670, and PNK7980) of the Korea Institute of Materials Science (KIMS) and the National Research Foundation of Korea (NRF) grants funded by the Korean government (Ministry of Science and ICT) (no. 2020M3D1A2081625).

REFERENCES

(1) Schmuch, R.; Wagner, R.; Hörpel, G.; Placke, T.; Winter, M. Performance and Cost of Materials for Lithium-based Rechargeable Automotive Batteries. *Nat. Energy* **2018**, *3*, 267−278.

(2) Miao, Y.; Hynan, P.; von Jouanne, A.; Yokochi, A. Current Li-Ion Battery Technologies in Electric Vehicles and Opportunities for Advancements. *Energies* **2019**, *12*, 1074.

(3) Quinn, J. B.; Waldmann, T.; Richter, K.; Kasper, M.; Wohlfahrt-Mehrens, M. Energy Density of Cylindrical Li-Ion Cells: A Comparison of Commercial 18650 to the 21700 Cells. *J. Electrochem. Soc.* **2018**, *165*, A3284−A3291.

(4) Lain, M. J.; Brandon, J.; Kendrick, E. Design Strategies for High Power vs. High Energy Lithium Ion Cells. *Batteries* **2019**, *5*, 64.

(5) Saw, L. H.; Ye, Y.; Tay, A. A. O. Electro-Thermal Analysis and Integration Issues of Lithium Ion Battery for Electric Vehicles. *Appl. Energy* **2014**, *131*, 97−107.

(6) Ren, X.; Li, Z.; Tian, W.; Zheng, Y.; Sun, J.; An, L.; Wang, F.; Wen, L.; Wang, X.; Wang, L.; Liang, G. Enhanced Cycling Performance of Cylindrical Lithium-Ion Battery with High Areal Capacity Electrodes via Non-uniform Load. *Ionics* **2020**, *26*, 691−702.

(7) Wang, L.; Yin, S.; Yu, Z.; Wang, Y.; Yu, T. X.; Zhao, J.; Xie, Z.; Li, Y.; Xu, J. Unlocking the Significant Role of Shell Material for Lithium-Ion Battery Safety. *Mater. Des.* **2018**, *160*, 601−610.

(8) Reynier, Y.; Vincens, C.; Leys, C.; Amestoy, B.; Mayousse, E.; Chavillon, B.; Blanc, L.; Gutel, E.; Porcher, W.; Hirose, T.; Matsui, C. Practical Implementation of Li Doped SiO in High Energy Density 21700 Cell. *J. Power Sources* **2020**, *450*, 227699.

(9) Xing, H.; Liu, Y.; Wang, B. Mechano-Electrochemical Analysis in Cylindrical Composition-Gradient Electrodes with Varying Young's Modulus of Lithium-Ion Battery. *J. Electrochem. Soc.* **2019**, *166*, A762−A770.

(10) Cao, J.; Luo, M.; Fang, X.; Ling, Z.; Zhang, Z. Liquid Cooling with Phase Change Materials for Cylindrical Li-Ion Batteries: An Experimental and Numerical Study. *Energy* **2020**, *191*, 116565.

(11) Park, K.; Yeon, D.; Kim, J. H.; Park, J.-H.; Doo, S.; Choi, B. Spinel-Embedded Lithium-Rich Oxide Composites for Li-Ion Batteries. *J. Power Sources* **2017**, *360*, 453−459.

(12) Makimura, Y.; Sasaki, T.; Nonaka, T.; Nishimura, Y. F.; Uyama, T.; Okuda, C.; Itou, Y.; Takeuchi, Y. Factors Affecting Cycling Life of $LiNi_{0.8}Co_{0.15}Al_{0.05}O_2$ for Lithium-Ion Batteries. *J. Mater. Chem. A* **2016**, *4*, 8350−8358.

(13) Waldmann, T.; Scurtu, R.-G.; Richter, K.; Wohlfahrt-Mehrens, M. 18650 vs. 21700 Li-ion cells − A Direct Comparison of Electrochemical, Thermal, and Geometrical Properties. *J. Power Sources* **2020**, *472*, 228614.

(14) Qian, G.; Liao, X.; Zhu, Y.; Pan, F.; Chen, X.; Yang, Y. Designing Flexible Lithium-Ion Batteries by Structural Engineering. *ACS Energy Lett.* **2019**, *4*, 690−701.

(15) Fang, Z.; Wang, J.; Wu, H.; Li, Q.; Fan, S.; Wang, J. Progress and Challenges of Flexible Lithium Ion Batteries. *J. Power Sources* **2020**, *454*, 227932.

(16) Chen, H.; Ling, M.; Hencz, L.; Ling, H. Y.; Li, G.; Lin, Z.; Liu, G.; Zhang, S. Exploring Chemical, Mechanical, and Electrical Functionalities of Binders for Advanced Energy-Storage Devices. *Chem. Rev.* **2018**, *118*, 8936−8982.

(17) Lee, H.; Yoo, J.-K.; Park, J.-H.; Kim, J. H.; Kang, K.; Jung, Y. S. A Stretchable Polymer−Carbon Nanotube Composite Electrode for Flexible Lithium-Ion Batteries: Porosity Engineering by Controlled Phase Separation. *Adv. Energy Mater.* **2012**, *2*, 976−982.

(18) Kumar, R.; Shin, J.; Yin, L.; You, J.-M.; Meng, Y. S.; Wang, J. All-Printed, Stretchable Zn-Ag_2O Rechargeable Battery via Hyperelastic Binder for Self-Powering Wearable Electronics. *Adv. Energy Mater.* **2017**, *7*, 1602096.

(19) Mackanic, D. G.; Yan, X.; Zhang, Q.; Matsuhisa, N.; Yu, Z.; Jiang, Y.; Manika, T.; Lopez, J.; Yan, H.; Liu, K.; Chen, X.; Cui, Y.; Bao, Z. Decoupling of Mechanical Properties and Ionic Conductivity in Supramolecular Lithium Ion Conductors. *Nat. Commun.* **2019**, *10*, 5384.

(20) Choi, S.; Kwon, T.-w.; Coskun, A.; Choi, J. W. Highly Elastic Binders Integrating Polyrotaxanes for Silicon Microparticle Anodes in Lithium Ion Batteries. *Science* **2017**, *357*, 279.

(21) Baughman, R. H.; Zakhidov, A. A.; de Heer, W. A. Carbon Nanotubes–the Route Toward Applications. *Science* **2002**, *297*, 787.

(22) Bauhofer, W.; Kovacs, J. Z. A Review and Analysis of Electrical Percolation in Carbon Nanotube Polymer Composites. *Compos. Sci. Technol.* **2009**, *69*, 1486−1498.

(23) Lekawa-Raus, A.; Patmore, J.; Kurzepa, L.; Bulmer, J.; Koziol, K. Electrical Properties of Carbon Nanotube Based Fibers and Their Future Use in Electrical Wiring. *Adv. Funct. Mater.* **2014**, *24*, 3661−3682.

(24) Napolskiy, F.; Avdeev, M.; Yerdauletov, M.; Ivankov, O.; Bocharova, S.; Ryzhenkova, S.; Kaparova, B.; Mironovich, K.; Burlyaev, D.; Krivchenko, V. On the Use of Carbon Nanotubes in Prototyping the High Energy Density Li-ion Batteries. *Energy Technol.* **2020**, *8*, 2000146.

(25) Yamazaki, S.; Yoshida, M.; Narita, T.; Kimura, K.; Morizawa, Y.; Yamamoto, I.; Inagi, S.; Fujimori, A.; Allcock, H. R.; Kaspar, H. *Fluorinated Polymers: Volume 2: Applications*. Royal Society of Chemistry: 2016.

(26) Zhou, Y.; Azumi, R.; Shimada, S. A Highly Durable, Stretchable, Transparent and Conductive Carbon Nanotube−Polymeric Acid Hybrid Film. *Nanoscale* **2019**, *11*, 3804−3813.

(27) Kharissova, O. V.; Kharisov, B. I.; de Casas Ortiz, E. G. Dispersion of Carbon Nanotubes in Water and Non-aqueous Solvents. *RSC Adv.* **2013**, *3*, 24812−24852.

(28) Pramanik, C.; Gissinger, J. R.; Kumar, S.; Heinz, H. Carbon Nanotube Dispersion in Solvents and Polymer Solutions: Mechanisms, Assembly, and Preferences. *ACS Nano* **2017**, *11*, 12805−12816.

(29) Ntim, S. A.; Sae-Khow, O.; Witzmann, F. A.; Mitra, S. Effects of Polymer Wrapping and Covalent Functionalization on the Stability of MWCNT in Aqueous Dispersions. *J. Colloid Interface Sci.* **2011**, *355*, 383−388.

(30) Verge, P.; Peeterbroeck, S.; Bonnaud, L.; Dubois, P. Investigation on the Dispersion of Carbon Nanotubes in Nitrile Butadiene Rubber: Role of Polymer-to-Filler Grafting Reaction. *Compos. Sci. Technol.* **2010**, *70*, 1453−1459.

(31) Sohrabi, B.; Poorgholami-Bejarpasi, N.; Nayeri, N. Dispersion of Carbon Nanotubes Using Mixed Surfactants: Experimental and Molecular Dynamics Simulation Studies. *J. Phys. Chem. B* **2014**, *118*, 3094−3103.

(32) Matsuzawa, Y.; Kato, H.; Ohyama, H.; Nishide, D.; Kataura, H.; Yoshida, M. Photoinduced Dispersibility Tuning of Carbon Nanotubes by a Water-Soluble Stilbene as a Dispersant. *Adv. Mater.* **2011**, *23*, 3922−3925.

(33) Valentini, L.; Bittolo Bon, S.; Hernández, M.; Lopez-Manchado, M. A.; Pugno, N. M. Nitrile Butadiene Rubber Composites Reinforced with Reduced Graphene Oxide and Carbon Nanotubes Show Superior Mechanical, Electrical and Icephobic Properties. *Compos. Sci. Technol.* **2018**, *166*, 109−114.

(34) Srivastava, S.; Mishra, Y. Nanocarbon Reinforced Rubber Nanocomposites: Detailed Insights about Mechanical, Dynamical Mechanical Properties, Payne, and Mullin Effects. *Nanomaterials* **2018**, *8*, 945.

(35) Verdier, N.; El Khakani, S.; Lepage, D.; Prébé, A.; Aymé-Perrot, D.; Dollé, M.; Rochefort, D. Polyacrylonitrile-based Rubber (HNBR) as a New Potential Elastomeric Binder for Lithium-Ion Battery Electrodes. *J. Power Sources* **2019**, *440*, 227111.

(36) Saha, S.; Bhowmick, A. K. Effect of Structure Development on the Rheological Properties of PVDF/HNBR-based Thermoplastic Elastomer and Its Vulcanizates. *J. Appl. Polym. Sci.* **2020**, *137*, 48758.

(37) Wang, Q. Robust and Thermal-Enhanced Melamine Formaldehyde−Modified Glassfiber Composite Separator for High-Performance Lithium Batteries. *Electrochim. Acta* **2015**, *182*, 334−341.

(38) Wang, Q.; Yu, Y.; Ma, J.; Zhang, N.; Zhang, J.; Liu, Z.; Cui, G. Electrospun Melamine Resin-based Multifunctional Nonwoven

https://doi.org/10.1021/acsami.1c00848
ACS Appl. Mater. Interfaces 2021, 13, 19970−19982

Membrane for Lithium Ion Batteries at the Elevated Temperatures. *J. Power Sources* **2016**, *327*, 196−203.
(39) Sui, Z.-Y.; Wang, C.; Yang, Q.-S.; Shu, K.; Liu, Y.-W.; Han, B.-H.; Wallace, G. G. A Highly Nitrogen-doped Porous Graphene − An Anode Material for Lithium Ion Batteries. *J. Mater. Chem. A* **2015**, *3*, 18229−18237.
(40) Fiset, E.; Rufford, T. E.; Seredych, M.; Bandosz, T. J.; Hulicova-Jurcakova, D. Comparison of Melamine Resin and Melamine Network as Precursors for Carbon Electrodes. *Carbon* **2015**, *81*, 239−250.
(41) Rodrigo, L.; Pou, P.; Martínez-Casado, R.; Martínez-Galera, A. J.; Gómez-Rodríguez, J. M.; Pérez, R. Characterizing Self-Assembled Molecular Layers on Weakly Interacting Substrates: the Role of Van Der Waals and the Chemical Interactions. *Nano Futures* **2018**, *2*, No. 045002.
(42) Hynes, L.; Montiel, G.; Jones, A.; Riel, D.; Abdulaziz, M.; Viva, F.; Bonetta, D.; Vreugdenhil, A.; Trevani, L. Melamine Adsorption on Carbon Materials: Impact of Carbon Texture and Surface Chemistry. *Mater. Adv.* **2020**, *1*, 262−270.
(43) Bauer, W.; Nötzel, D. Rheological Properties and Stability of NMP Based Cathode Slurries for Lithium Ion Batteries. *Ceram. Int.* **2014**, *40*, 4591−4598.
(44) Hansen, M. R.; Graf, R.; Spiess, H. W. Interplay of Structure and Dynamics in Functional Macromolecular and Supramolecular Systems As Revealed by Magnetic Resonance Spectroscopy. *Chem. Rev.* **2016**, *116*, 1272−1308.
(45) Gao, Y.; Liu, S.; Wang, Q.; Wang, G. Preparation of Melamine−Formaldehyde Resin Grafted by (3-aminopropyl) triethoxysilane for High-Performance Hydrophobic Materials. *J. Appl. Polym. Sci.* **2020**, *137*, 48664.
(46) Choi, W.; Lim, N.; Choi, H.; Seo, M.; Ahn, J.; Jung, J. Self-Assembled Triphenylphosphonium-Conjugated Dicyanostilbene Nanoparticles and Their Fluorescence Probes for Reactive Oxygen Species. *Nanomaterials* **2018**, *8*, 1034.
(47) Nalluri, S. K. M.; Liu, Z.; Wu, Y.; Hermann, K. R.; Samanta, A.; Kim, D. J.; Krzyaniak, M. D.; Wasielewski, M. R.; Stoddart, J. F. Chiral Redox-Active Isosceles Triangles. *J. Am. Chem. Soc.* **2016**, *138*, 5968−5977.
(48) Hester, J. F.; Banerjee, P.; Won, Y. Y.; Akthakul, A.; Acar, M. H.; Mayes, A. M. ATRP of Amphiphilic Graft Copolymers Based on PVDF and Their Use as Membrane Additives. *Macromolecules* **2002**, *35*, 7652−7661.
(49) Fujiwara, H.; Ono, H.; Nishimura, S. Degradation behavior of acrylonitrile butadiene rubber after cyclic high-pressure hydrogen exposure. *Int. J. Hydrogen Energy* **2015**, *40*, 2025−2034.
(50) Liu, J.; Sun, J.; Zhang, Z.; Yang, H.; Nie, X. One-step Synthesis of End-Functionalized Hydrogenated Nitrile-Butadiene Rubber by Combining the Functional Metathesis with Hydrogenation. *ChemistryOpen* **2020**, *9*, 374−380.
(51) Cai, X.; Lei, T.; Sun, D.; Lin, L. A Critical Analysis of the α, β and γ Phases in Poly(vinylidene fluoride) Using FTIR. *RSC Adv.* **2017**, *7*, 15382−15389.
(52) Wu, T.; Zhou, B.; Zhu, T.; Shi, J.; Xu, Z.; Hu, C.; Wang, J. Facile and Low-Cost Approach towards a PVDF Ultrafiltration Membrane with Enhanced Hydrophilicity and Antifouling Performance via Graphene Oxide/Water-Bath Coagulation. *RSC Adv.* **2015**, *5*, 7880−7889.
(53) Ren, Y.; Wang, Y.; Zhang, W.; Yan, X.; Huang, B. Improved Battery Performance Contributed by the Optimized Phase Ratio of β and α of PVDF. *RSC Adv.* **2019**, *9*, 29760−29764.
(54) Dementjev, A. P.; de Graaf, A.; van de Sanden, M. C. M.; Maslakov, K. I.; Naumkin, A. V.; Serov, A. A. X-Ray Photoelectron Spectroscopy Reference Data for Identification of the C_3N_4 Phase in Carbon−Nitrogen Films. *Diamond Relat. Mater.* **2000**, *9*, 1904−1907.
(55) Pérez-Luna, V.; Moreno-Aguilar, C.; Arauz-Lara, J. L.; Aranda-Espinoza, S.; Quintana, M. Interactions of Functionalized Multi-Wall Carbon Nanotubes with Giant Phospholipid Vesicles as Model Cellular Membrane System. *Sci. Rep.* **2018**, *8*, 17998.
(56) Vandencasteele, N.; Reniers, F. Plasma-modified Polymer Surfaces: Characterization using XPS. *J. Electron Spectrosc.* **2010**, *178-179*, 394−408.
(57) Yoo, J.-K.; Oh, Y.; Park, T.; Lee, K. E.; Um, M.-K.; Yi, J.-W. Optimization of Carbon Nanotubes as Conductive Additives for High-Energy-Density Electrodes for Lithium-Ion Batteries. *Energy Technol.* **2019**, *7*, 1800845.
(58) Kim, D. W.; Hwang, S. M.; Yoo, J. B.; Kim, Y.-J. Electrode Engineering with CNTs to Enhance the Electrochemical Performance of $LiNi_{0.6}Co_{0.2}Mn_{0.2}O_2$ Cathodes with Commercial Level Design Parameters. *ChemElectroChem* **2020**, *7*, 2621.
(59) Wang, B.; Jeon, Y. S.; Bhang, S. H.; Kim, J. H. Bioinspired Dopamine-Conjugated Polyaspartamide as a Novel and Versatile Adhesive Material. *Express Polym. Lett.* **2017**, *11*, 601−610.
(60) Pieczonka, N. P. W.; Borgel, V.; Ziv, B.; Leifer, N.; Dargel, V.; Aurbach, D.; Kim, J.-H.; Liu, Z.; Huang, X.; Krachkovskiy, S. A.; Goward, G. R.; Halalay, I.; Powell, B. R.; Manthiram, A. Lithium Polyacrylate (LiPAA) as an Advanced Binder and a Passivating Agent for High-Voltage Li-Ion Batteries. *Adv. Energy Mater.* **2015**, *5*, 1501008.
(61) Tebbe, J. L.; Fuerst, T. F.; Musgrave, C. B. Mechanism of hydrofluoric acid formation in ethylene carbonate electrolytes with fluorine salt additives. *J. Power Sources* **2015**, *297*, 427−435.
(62) Rajak, S.; Chair, K.; Rana, L. K.; Kaur, P.; Maris, T.; Duong, A. Amidine/Amidinate Cobalt Complexes: One-Pot Synthesis, Mechanism, and Photocatalytic Application for Hydrogen Production. *Inorg. Chem.* **2020**, *59*, 14910−14919.
(63) Yang, X.; Lin, M.; Zheng, G.; Wu, J.; Wang, X.; Ren, F.; Zhang, W.; Liao, Y.; Zhao, W.; Zhang, Z.; Xu, N.; Yang, W.; Yang, Y. Enabling Stable High-Voltage $LiCoO_2$ Operation by Using Synergetic Interfacial Modification Strategy. *Adv. Funct. Mater.* **2020**, *30*, 2004664.
(64) Bredar, A. R. C.; Chown, A. L.; Burton, A. R.; Farnum, B. H. Electrochemical Impedance Spectroscopy of Metal Oxide Electrodes for Energy Applications. *ACS Appl. Energy Mater.* **2020**, *3*, 66−98.
(65) Xu, M.; Zhou, L.; Dong, Y.; Chen, Y.; Garsuch, A.; Lucht, B. L. Improving the Performance of Graphite/ $LiNi_{0.5}Mn_{1.5}O_4$Cells at High Voltage and Elevated Temperature with Added Lithium Bis(oxalato) Borate (LiBOB). *J. Electrochem. Soc.* **2013**, *160*, A2005−A2013.
(66) Zhou, P.; Jiang, L.; Wang, F.; Deng, K.; Lv, K.; Zhang, Z. High performance of a cobalt−nitrogen complex for the reduction and reductive coupling of nitro compounds into amines and their derivatives. *Sci. Adv.* **2017**, *3*, No. e1601945.
(67) Li, Q.; Qiao, R.; Wray, L. A.; Chen, J.; Zhuo, Z.; Chen, Y.; Yan, S.; Pan, F.; Hussain, Z.; Yang, W. Quantitative probe of the transition metal redox in battery electrodes through soft x-ray absorption spectroscopy. *J. Phys. D: Appl. Phys.* **2016**, *49*, 413003.

https://doi.org/10.1021/acsami.1c00848
ACS Appl. Mater. Interfaces 2021, 13, 19970−19982